Supporting Information

HKUST-1 Metal-Organic Framework Nanoparticle/Graphene Oxide Nanocomposite Aerogels for CO_2 and CH_4 Adsorption and Separation

Albert Rosado,[1] Alejandro Borrás,[1] Julio Fraile,[1] Jorge A. R. Navarro,[2] Fabián Suárez-García,[3] Kyriakos C. Stylianou,[4] Ana M. López-Periago,[1] José Giner Planas,[1,*] Concepción Domingo,[1,*] Amirali Yazdi[1,*]

Author Information:

Albert Rosado: Materials Science Institute of Barcelona, ICMAB-CSIC, Campus UAB s/n, 08193, Barcelon, Spain. Email: arosado@icmab.es

Alejandro Borrás: Instituto de Ciencia de Materiales de Barcelona, ICMAB-CSIC, Campus UAB s/n, 08193, Barcelon, Spain. Email: aborras@icmab.es

Julio Fraile: Instituto de Ciencia de Materiales de Barcelona, ICMAB-CSIC, Campus UAB s/n, 08193, Barcelon, Spain. Email: julio@icmab.es

Jorge A. R. Navarro: Departamento de Química Inorgánica, Universidad de Granada, Av. Fuentenueva S/N, 18071, Granada, Spain. Email: jarn@ugr.es

Fabián Suárez-García: Instituto de Ciencia y Tecnología del Carbono, INCAR-CSIC, C/Francisco Pintado Fe 26, 33011, Oviedo, Spain. Email: fabian@incar.csic.es

Kyriakos C. Stylianou: Department of Chemistry, Oregon State University, Corvallis, OR 97331, USA kyriakos.stylianou@oregonstate.edu

Ana M. López-Periago: Instituto de Ciencia de Materiales de Barcelona, ICMAB-CSIC, Campus UAB s/n, 08193, Barcelon, Spain. Email: amlopez@icmab.es

José Giner Planas: Instituto de Ciencia de Materiales de Barcelona, ICMAB-CSIC, Campus UAB s/n, 08193, Barcelon, Spain. Email: jginerplanas@icmab.es. Corresponding author

Concepción Domingo: Instituto de Ciencia de Materiales de Barcelona, ICMAB-CSIC, Campus UAB s/n, 08193, Barcelon, Spain. Email: conchi@icmab.es. Corresponding author

Amirali Yazdi: Instituto de Ciencia de Materiales de Barcelona, ICMAB-CSIC, Campus UAB s/n, 08193, Barcelon, Spain. Email: amirali.yazdi@yahoo.com. Corresponding author

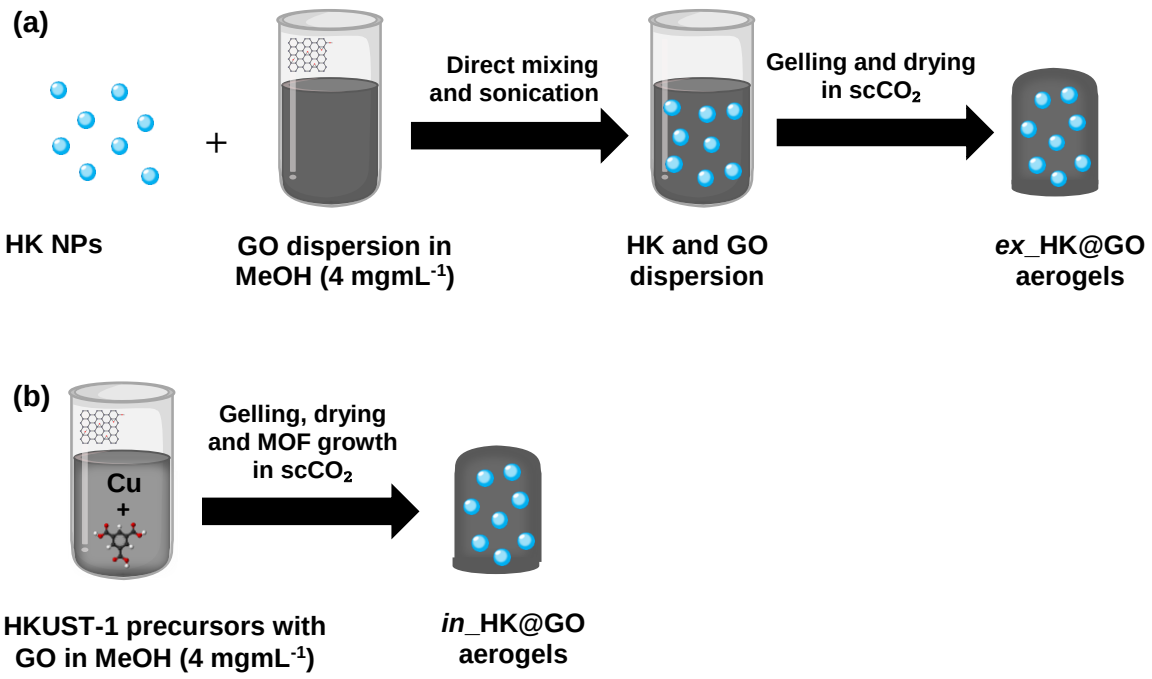

Figure S1. Schematic representation of the synthetic steps used to obtain HKUST-1@GO nanocomposite aerogels by: (a) *ex situ* (*ex*_HK@GO), and (b) *in situ* (*in*_HK@GO) protocols and $scCO_2$ drying.

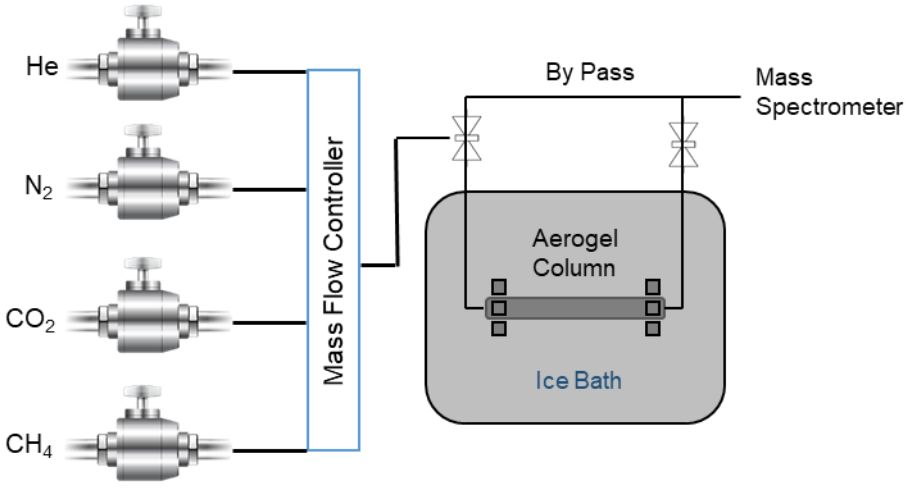

Figure S2. Scheme of the system employed for running dynamic breakthrough experiments.

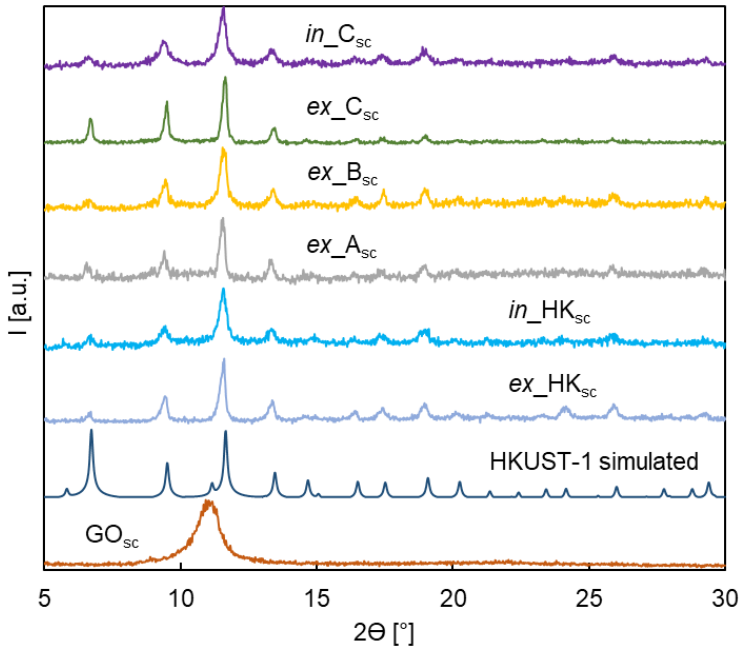

Figure S3. XRD patterns for the different studied samples.

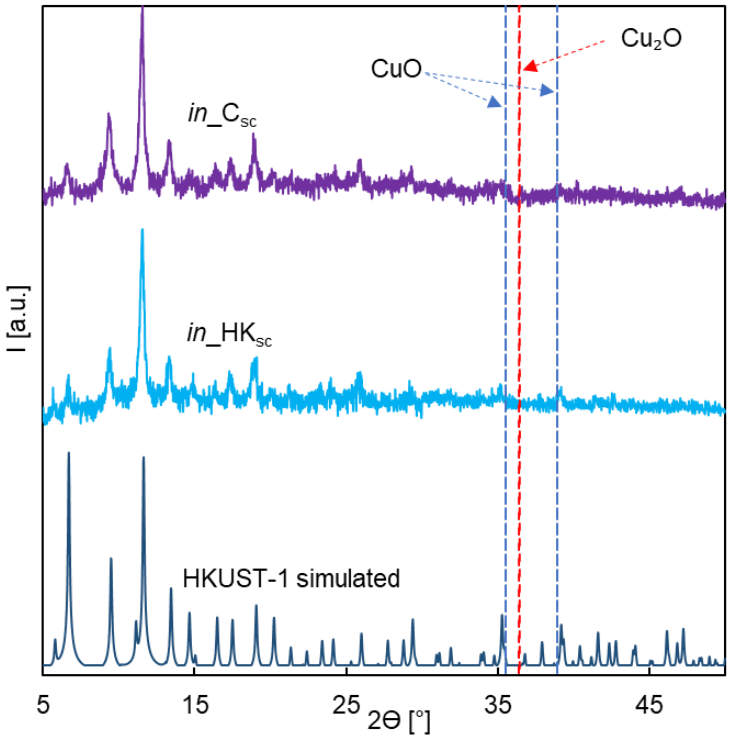

Figure S4. XRD patterns for the precipitated *in situ* samples in the 2Θ range 5-50º. Dashed lines indicate the location of the most intense XRD bands assigned to CuO and Cu_2O.

TGA description (Fig. S5). For GO_{sc} aerogel, a first mass decay (*ca.* 5 wt%) was observed below 423 K that is attributed to the evaporation of weakly adsorbed water. Then, the decomposition of GO_{sc} occurred in two steps: a gradual decay (*ca.* 448-523 K), assigned to the loss of oxygenated groups (*ca.* 30 wt%); and a final abrupt weight loss between 648 and 698 K, attributed to the combustion of graphene in air. For *ex*_HK_{sc}, the first mass loss stages up to *ca.* 448 K is ascribed to the evaporation of adsorbed water incorporated to the sample during manipulation. Next, the profile showed the decomposition of the MOF at 280 K, occurring by combustion of BTC moieties and resulting in the formation of CuO. For sample *ex*_B_{sc}, the weight loss below 398 K was attributed to the evaporation of weakly adsorbed water. Next, the decay of weight in the interval 448-523 K was assigned to the presence of oxygenated groups (hydroxyl and epoxy) in the GO component. The collapse of the structure of HKUST-1 in the composite arises, as for ex_HK_{sc}, at 553 K. The composite did not lose any further weight, signifying that the pyrolysis of GO likely occurred at the same time than HKUST-1 decomposition, because of the large exothermic effects associated with the oxidation (burning) of the organic linker in the MOF.

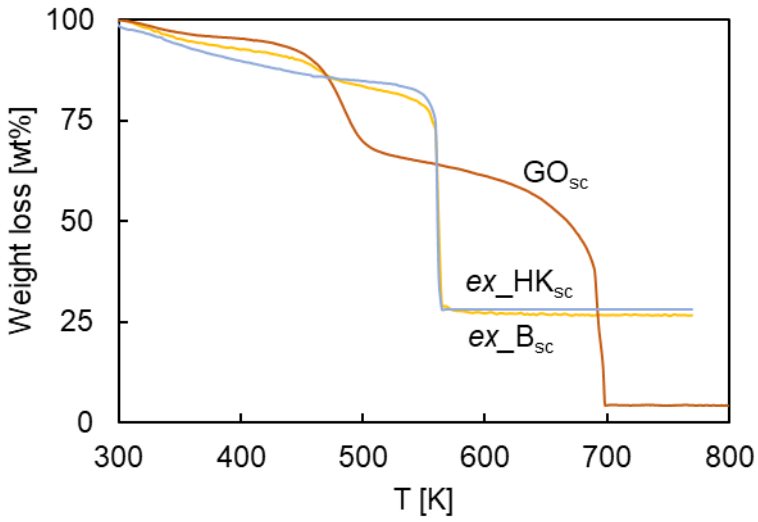

Figure S5. TGA profiles measured in air for the composite *ex*_B_{sc} and its composing products.

ATR-FTIR analysis (Fig. S6). For the GO_{sc} sample, the broad signal centered at 3290 cm^{-1} is typical of the O-H stretching mode of the hydroxyls on the GO flakes surface. The incipient signals at 2857 and 2924 cm^{-1} correspond to methylene symmetric and asymmetric stretching modes in the graphene network. The weak signal at 1724 cm^{-1} is attributed to the stretching mode of C=O bond, indicating only little density of carbonyl and carboxyl functionalities throughout the network. The signal at 1631 cm^{-1} is constituted by the overlapping of two peaks produced by the O-H and the C=C in plane bending. The signal at 1373 cm^{-1} arises from the C-OH stretching mode, whereas the peak at 1229 cm^{-1} comes from the C-O-C stretching mode. The peak at 1060 cm^{-1} is attributed to C-O bond stretching coming from both alkoxy and epoxy.[1] For HKUST-1 and composite samples, the peak at 1649 cm^{-1} corresponds to the C=O stretching mode of carboxylic acids in BTC, as well as the peaks at 1449 and 1372 cm^{-1} that correspond to ring vibration and C-O stretching mode, respectively. Moreover, the small signal at 941 cm^{-1} is assigned to C-H in plane bending. The signal at 1110 cm^{-1} is due to C-O-Cu stretching. The sharp peaks at 727 and 760 cm^{-1} correspond to the vibration of the aromatic ring when Cu(II) ions are coordinated.[2]

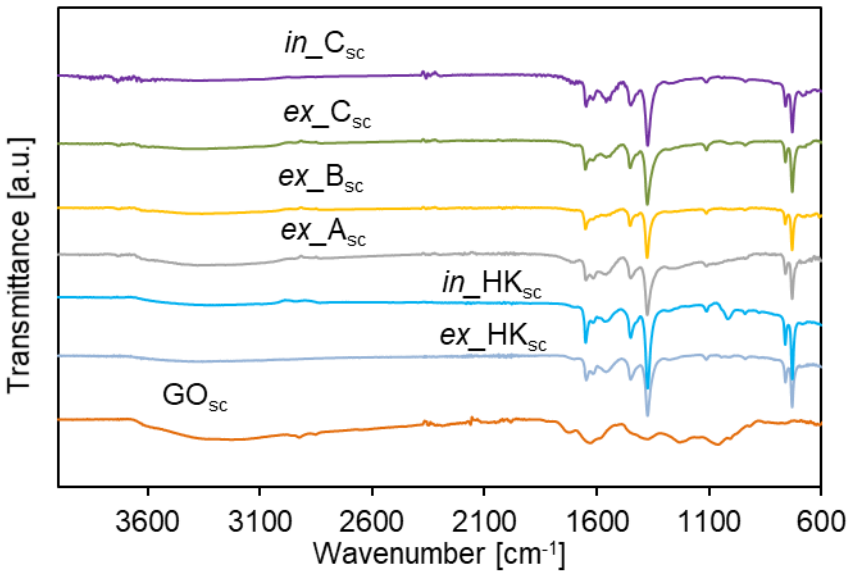

Figure S6. ATR-FTIR spectra of the studied composites and composing units.

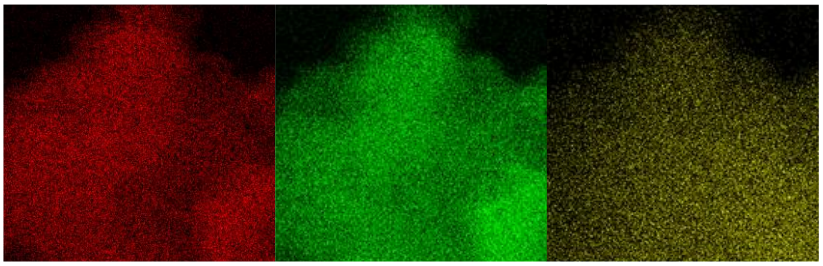

Figure S7. EDS analysis of sample *ex*_C_{sc} performed on a SEM backscattered image, representing the elements C (red), O (green) and Cu (yellow).

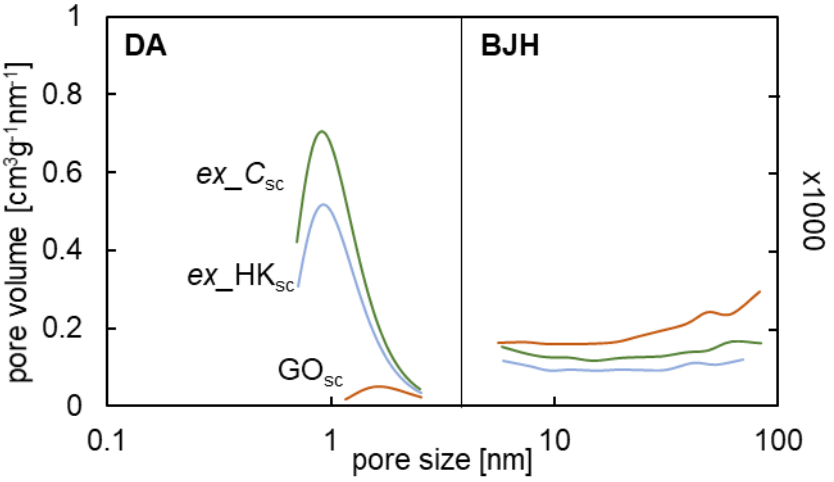

Figure S8. Dubinin-Astakhov (DA) and Barrett-Joyner-Halenda (BJH) plots of volumetric pore size distribution for *ex situ ex*_C_{sc} nanocomposite and composing units.

Table S1. Summary of the textural properties of the studied samples and comparison with their analogs calculated physical mixtures.

Sample	Sa [$m^2\ g^{-1}$]	μSa [$m^2\ g^{-1}$]	mPv [$cm^3\ g^{-1}$]	μPv [$cm^3\ g^{-1}$]
*ex*_A_{sc}	760	555	0.29	0.22
*ex*_A_{pm}	635	390	0.41	0.15
*ex*_B_{sc}	1125	790	0.41	0.32
*ex*_B_{pm}	800	540	0.38	0.21
*ex*_C_{sc}	1520	1260	0.37	0.49
*ex*_C_{pm}	1045	765	0.35	0.29
*in*_C_{sc}	1140	870	0.84	0.34
*in*_C_{pm}	1070	815	0.83	0.32

Supercritically *vs.* air dried samples: kinetics of gas (N_2) diffusion

Unlike supercritically dried samples, the formation of a porous structure was hindered in the air dried *ex*_C_{ad} sample. Instead, the GO flakes analyzed by SEM were found stacked at the bottom of the flask as micro-sized bricks, entrapping spots of aggregated HKUST-1 NPs (Fig. S9a,b). The XRD pattern of the *ex*_C_{ad} sample revealed the presence of an incipient band at 2θ around 11º, corresponding to stacked GO flakes (Fig. S9c). Regarding N_2 adsorption, the *ex*_C_{sc} aerogel exhibits a type I isotherm at low p/p^0 and a type IV isotherm at medium p/p^0. Contrarily, the air dried composite *ex*_C_{ad} displayed a strictly type I isotherm, without any hysteresis at medium pressures denoting mesoporosity, and with significantly lower values of N_2 adsorption than the counterpart aerogel *ex*_C_{sc} (Fig. S9d). In the *ex*_C_{ad}, due to flakes staking, the mesoporosity was totally lost and, moreover, part of the HKUST-1 microporosity was blocked in the sandwich-

like structure becoming inaccessible for N_2 adsorption. This observation was verified by performing N_2 adsorption experiments at different (post-)equilibrium times in samples *ex*_C_{sc} and *ex*_C_{ad}, *e.g.*, 10 (routine) and 120 s (Fig. S9d). Two superimposed isotherms were obtained by measuring the aerogel *ex*_C_{sc} at both equilibrium intervals. Contrarily, a significant increase on the N_2 adsorption values of the isotherm recorded for *ex*_C_{ad} was observed by delaying to 120 s the measurement between two equilibrium points, which results in an increase of measured apparent micropore surface area and volume (Table S2).

Table S2. Summary of the textural properties of the ex_C_{sc} and *ex*_C_{ad} samples measured at 10 and 120 s equilibrium times.

Sample	**Sa** $[m^2g^{-1}]$	**µSa** $[m^2g^{-1}]$	**mPv** $[cm^3g^{-1}]$	**µPv** $[cm^3g^{-1}]$
*ex*_C_{sc} (10 s)	1520	1260	0.37	0.49
*ex*_C_{sc} (120 s)	1560	1310	0.35	0.51
*ex*_C_{ad} (10 s)	370	265	0.06	0.10
*ex*_C_{ad} (120 s)	500	385	0.06	0.15

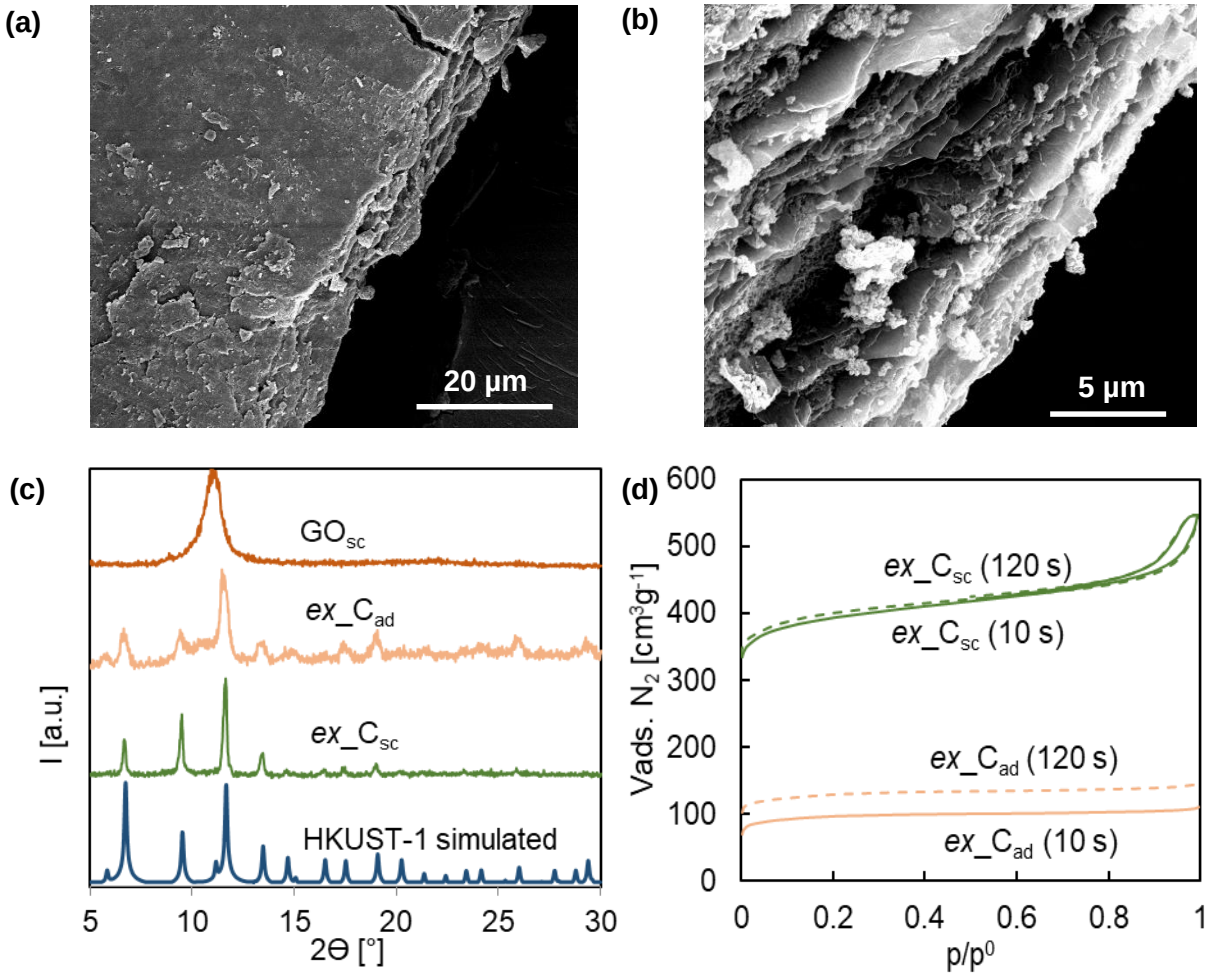

Figure S9. Characterization of the air dried *ex*_C_{ad} sample compared to *ex*_C_{sc}: (a) SEM micrograph of *ex*_C_{ad}, (b) XRD patterns, and N_2 isotherms at (c) 10 s and (d) 10 and 120 s.

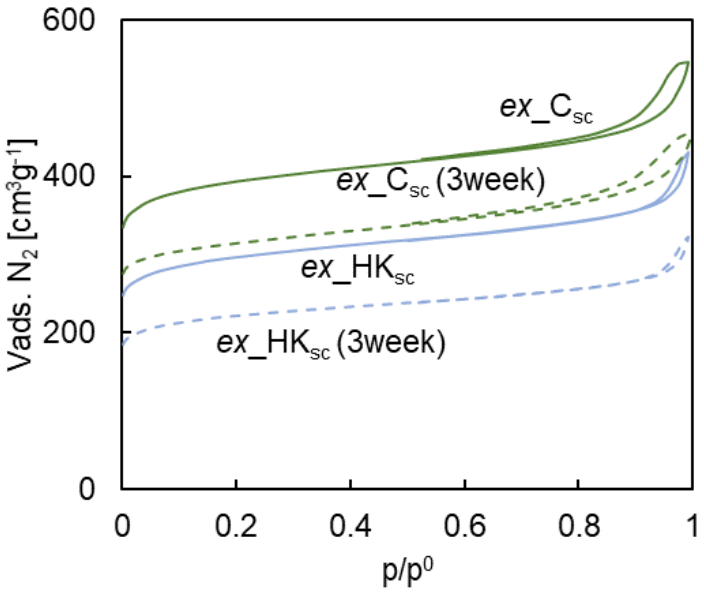

Figure S10. N_2 adsorption/desorption isotherms obtained for *ex*_HK_{sc} and *ex*_C_{sc} as-synthetized samples and after exposing them to humidity for three weeks.

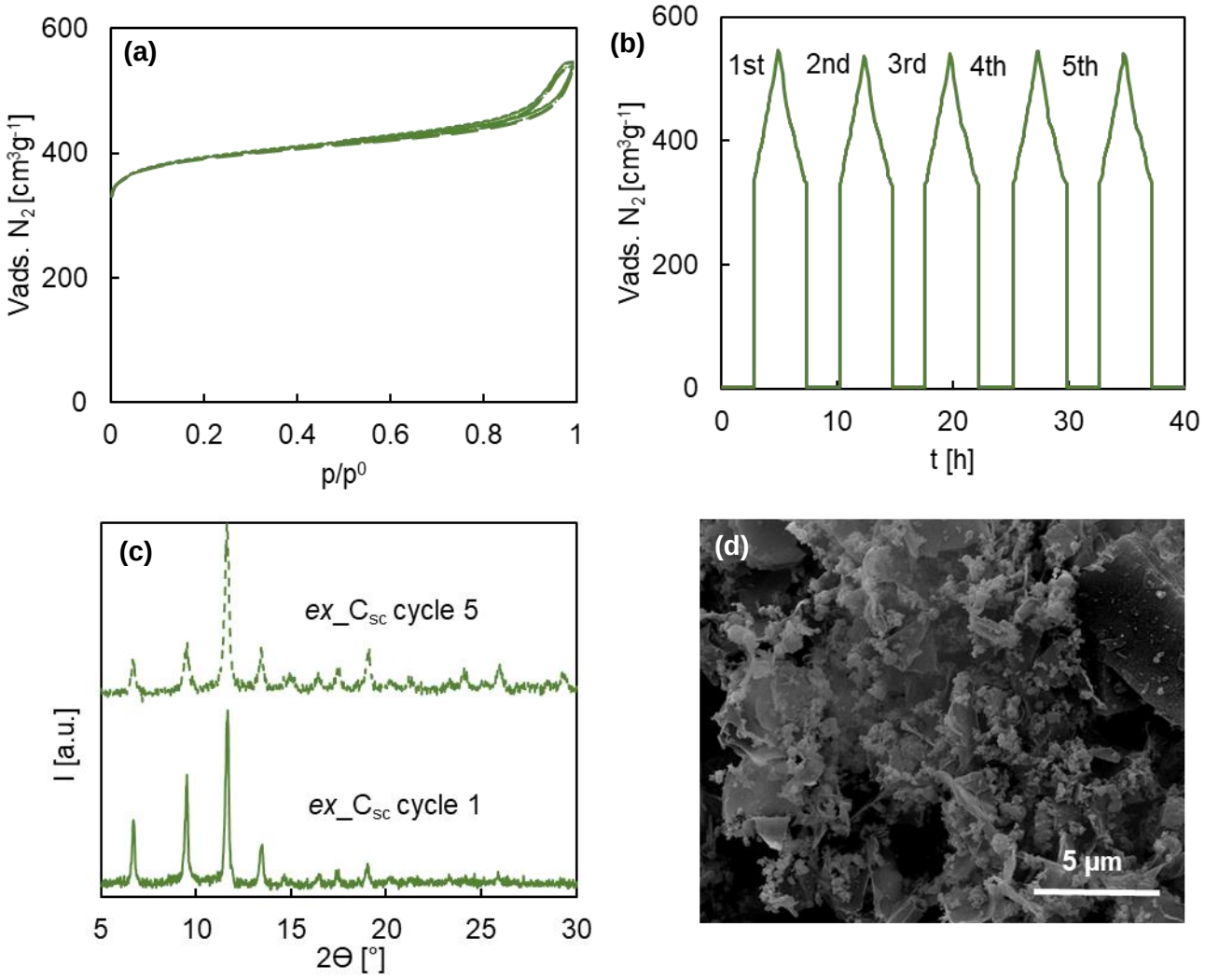

Figure S11. Characterization of sample *ex*_C_{sc} after repeating N_2 adsorption/desorption for five cycles: (a) isotherms, (b) evolution with time, (c) XRD pattern, and (d) SEM micrograph at cycle five.

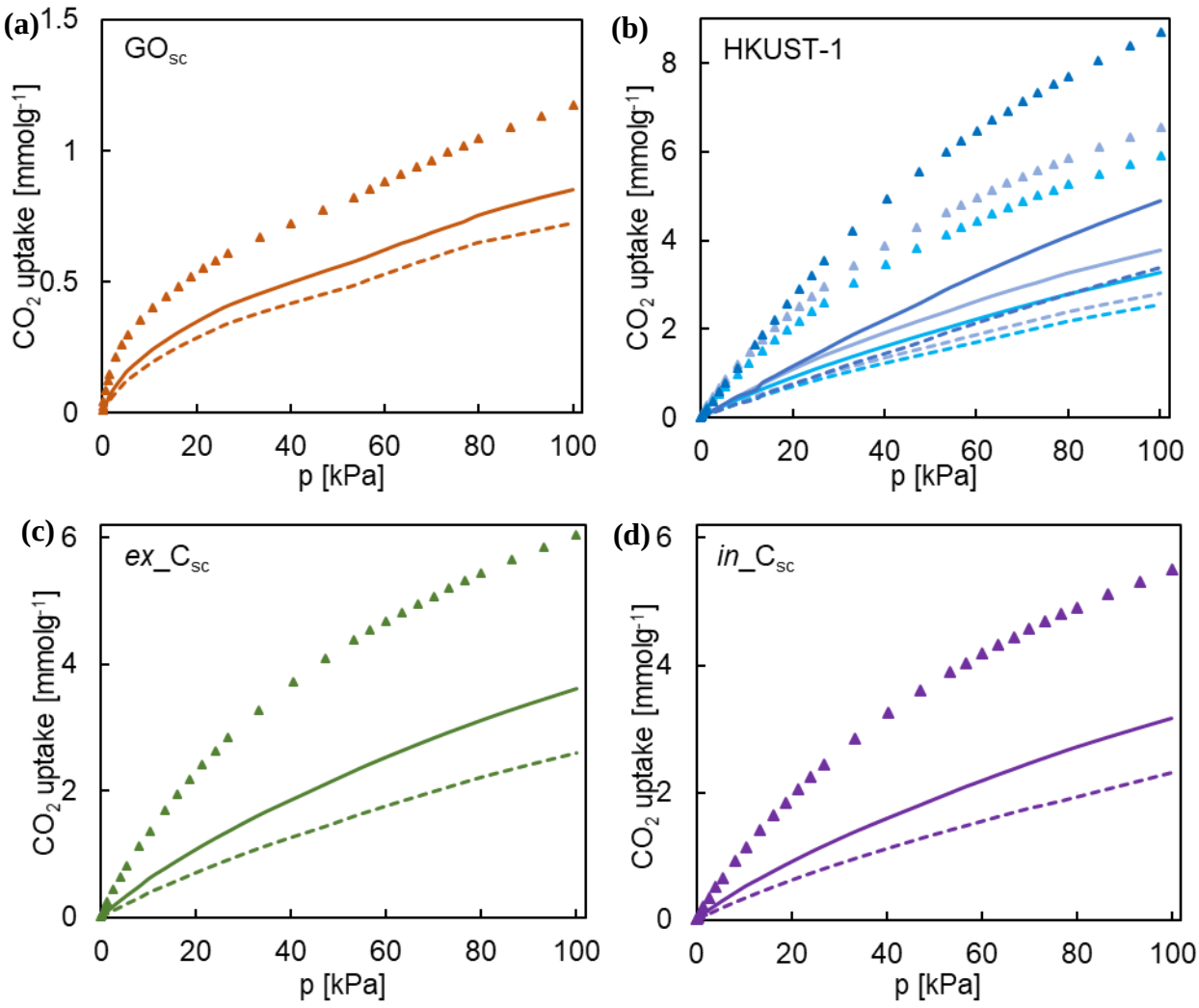

Figure S12. CO_2 adsorption isotherms at different temperatures for some representative studied products: (a) GO_{sc}, (b) HKUST-1 NPs (light blue *ex*_HK_{sc}, emerald blue *in*_HK_{sc}), (c) *ex*_C_{sc}, and (d) *in*_C_{sc}. Dotted line 313 K, straight line 298 K and triangles 273 K.

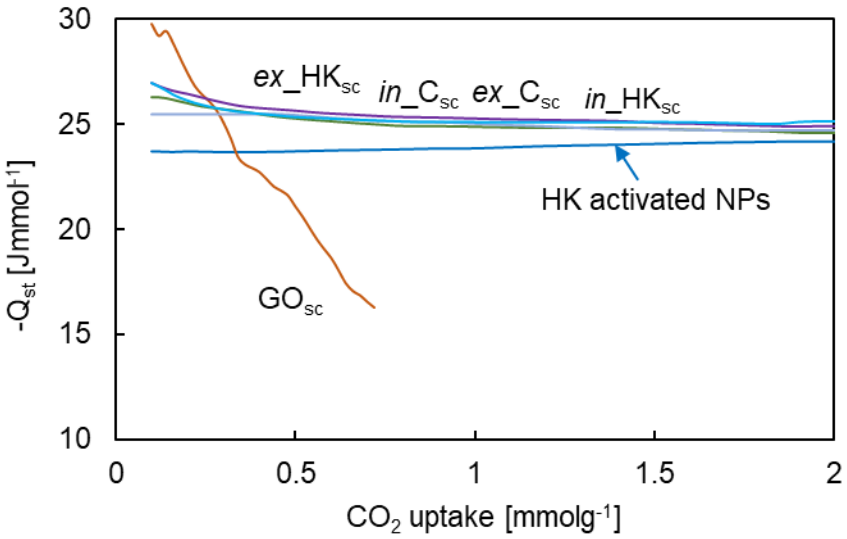

Figure S13. Isosteric heats of adsorption (Q_{st}) at different surface coverages of CO_2 for the different synthetized samples.

References

(1) Khalili, D. Graphene Oxide: A Promising Carbocatalyst for the Regioselective Thiocyanation of Aromatic Amines, Phenols, Anisols and Enolizable Ketones by Hydrogen Peroxide/KSCN in Water. *New J. Chem.* **2016**, *40* (3), 2547–2553. https://doi.org/10.1039/c5nj02314a.

(2) Yang, A.; Li, P.; Zhong, J. Facile Preparation of Low-Cost HKUST-1 with Lattice Vacancies and High-Efficiency Adsorption for Uranium. *RSC Adv.* **2019**, *9* (18), 10320–10325. https://doi.org/10.1039/c9ra01427f.